

Article

Shape Memory Properties and Microstructure of New Iron-Based FeNiCoAlTiNb Shape Memory Alloys

Li-Wei Tseng ^{1,*}, Chih-Hsuan Chen ², Wei-Cheng Chen ¹, Yu Cheng ² and Nian-Hu Lu ²

¹ Department of Mechatronics Engineering, National Changhua University of Education, Changhua 50007, Taiwan; earth520ya@gmail.com

² Department of Mechanical Engineering, National Taiwan University, Taipei 10617, Taiwan; chchen23@ntu.edu.tw (C.-H.C.); f06543027@ntu.edu.tw (Y.C.); f06522712@ntu.edu.tw (N.-H.L.)

* Correspondence: lwtseeng@cc.ncue.edu.tw

Abstract: The shape memory properties and microstructure of Fe₄₁Ni₂₈Co₁₇Al_{11.5}(Ti+Nb)_{2.5} (at.%) cold-rolled alloys were studied at the first time using the values reported in constant stress thermal cycling experiments in a three-point bending test. Thermo-magnetization curves of 97% cold-rolled and solution-treated sample aged at 600 °C for 24, 48 and 72 h showed evidence of the martensitic transformation, and the transformation temperatures increased their values from 24 to 72 h. The alloy cold-rolled to 97% and then solution-treated at 1277 °C for 1 h showed that most grains were aligned near <100> in the rolling direction in the recrystallization texture. The intensity of texture was 13.54, and an average grain size was around 400 μm. The sample aged at 600 °C for 48 h showed fully recoverable strain up to 1.6% at 200 MPa stress level in the three-point bending test. However, the experimental recoverable strain values were lower than the theoretical values, possibly due to the small volume fraction of low angle grain boundary, the formation of brittle grain boundary precipitates, and a grain boundary constraint lower than the expected intensity of texture in the samples.

Keywords: shape memory alloys; FeNiCoAlTiNb; microstructure; shape memory effect; martensitic transformation



Citation: Tseng, L.-W.; Chen, C.-H.; Chen, W.-C.; Cheng, Y.; Lu, N.-H. Shape Memory Properties and Microstructure of New Iron-Based FeNiCoAlTiNb Shape Memory Alloys. *Crystals* **2021**, *11*, 1253. <https://doi.org/10.3390/cryst11101253>

Academic Editor: Wojciech Polkowski

Received: 14 September 2021

Accepted: 13 October 2021

Published: 15 October 2021

Publisher's Note: MDPI stays neutral with regard to jurisdictional claims in published maps and institutional affiliations.



Copyright: © 2021 by the authors. Licensee MDPI, Basel, Switzerland. This article is an open access article distributed under the terms and conditions of the Creative Commons Attribution (CC BY) license (<https://creativecommons.org/licenses/by/4.0/>).

1. Introduction

Shape memory alloys (SMAs) are small materials with functional and intelligent properties. SMAs exhibit two unique properties: (i) the shape memory effect, in which the material can recover the deformation upon heating or magnetization, and (ii) superelasticity, which is stress-induced during martensitic transformation, and the material can recover the deformation after removing the load. Currently, nickel–titanium (NiTi) SMAs are the most well-developed SMAs and are commonly used in industries including aerospace, automotive, biomedical, robotics, actuators and sensors due to their high recoverable strain in both tension and compression [1–3]. However, the materials used in NiTi SMAs have a high cost and they have difficulty in cold rolling. These factors limit the applications of large quantities of NiTi SMAs due to the cost of materials and processing issues [4]. Compared to NiTi alloys, iron-based SMAs are commercially attractive because they have a low material cost and good machinability and workability. As a result, iron-based SMAs have attracted attention and interest in the industry and academic fields.

The martensitic transformation (MT) of Fe-based SMAs is classified into three groups based on their martensite and austenite structures: (1) face-centered cubic (FCC) (austenite) to body-centered cubic (BCC) or body-centered tetragonal (BCT) (martensite). This transformation system can be observed in an FeNi-based alloy system [5–10]. (2) The martensitic transformation in FeMnSi SMAs are FCC-HCP [11,12]: FCC (austenite) to hexagonal close-packed (HCP) (martensite). (3) The transformation system reported in FeMnAl [13], FeMnGa [14,15] and FeMnAlNi [16] SMAs is BCC (austenite) to FCC (martensite).

In general, four distinct morphologies of martensite in iron-based SMAs can be observed: lenticular, lath, butterfly and thin plate [1,17]. Lenticular martensite is formed in FePt SMAs. In FeNi alloys, thin plate martensite forms at the lowest temperature, lenticular martensite forms at intermediate temperatures and lath martensite forms at the highest temperature [17]. The formation of lath martensite typically contains a high density of internal dislocations due to accommodation distortion. Unlike the lath martensite, thin plate types of martensite contain a high density of transformation twins. For butterfly type of martensite, the substructure comprises a mixture of dislocations and twins [17]. Among four types of martensite morphology, only the thin plate martensite shows the shape memory effect [1].

Most Fe-based SMAs, such as FeMnAl, FeNiCoTi, FeMnSi and FeMnGa SMAs, show less than 1% recoverable strain of superelasticity [1,3,5,11,13]. Recently, two new Fe-based SMAs systems were presented, with superelastic strains above 4% at room temperature. The first system is Fe_{40.95}Ni₂₈Co₁₇Al_{11.5}Ta_{2.5}B_{0.05} (at.%), which shows a 13.5% superelastic strain [9], and in a similar system, FeNiCoAlXB (X: Ta, Nb, Ti) presents a 5% superelastic strain in polycrystalline alloys [9,10,18,19], single crystals [20–24] and wire [25]. The second system is Fe_{43.5}Mn₃₄Al₁₅Ni_{7.5} (at.%), and this system shows a 5% superelastic strain in polycrystalline alloys [16,26,27], polycrystalline wires [28–30] and single crystals [31,32]. In FeNiCoAlXB (X: Ta, Nb, Ti) alloy systems, three conditions are required to achieve this excellent superelastic property. (1) A strong texture is required in these alloys. If the texture is random, it shows brittle behavior. In FeNiCoAlTaB and FeNiCoAlTiB alloys, the strong texture is in the <100> orientation [8,10]. In FeNiCoAlNb alloys, the strong texture is in the <110> orientation [9]. (2) A large grain size is required to decrease the grain boundary and triple junction constraints during the superelastic tests. In FeNiCoAlTaB alloys, the average grain size is around 400 µm [8,33]. (3) The alloy is required to undergo aging heat treatment to obtain L₁₂ precipitates. The nano size precipitates not only strengthen the matrix but also change the material from non-thermoelastic to thermoelastic transformation [8]. The precipitate size is around 3 nm for the 600 °C–72 h sample [8].

Studies regarding the shape memory behavior of <100>-oriented Fe₄₁Ni₂₈Co₁₇Al_{11.5}Ta_{2.5} (at.%) single crystals have been carried out. Ma et al. [20] reported a 3.75% recoverable strain in tension at the stress level of 50 MPa. The precipitate size was around 5 nm for a 600 °C–90 h sample. Czerny et al. [34,35] found that two stages of aging heat treatment could improve the compressive properties. A FeNiCoAlTa single crystal underwent the first stage of aging at 700 °C for 0.5 h and the second stage of aging at 700 °C for 3 h, showing a 15% superelastic strain at –196 °C [35].

Tseng et al. [23] found that using Ti to replace Ta could reduce the aging heat treatment times. A FeNiCoAlTi single crystal with <100> orientation aged at 600 °C for 4 h possessed 6% superelastic strain when the test temperature was at –80 °C. Chumlyakov et al. [36–38] showed that adding Nb to this alloy could increase the hardness of the austenite matrix and improve their superelastic properties. FeNiCoAlNb single crystals with <100> orientation in two-step aging (700 °C–0.5 h + 700 °C–3 h) demonstrated 7% superelastic strain in tension and 13.5% in compression. The precipitates size ranged from 5 to 8 nm [38].

Poklonov et al. [39] reported <100>-oriented FeNiCoAlTiNb single crystals that underwent a thermal cycling tensile test and obtained 2.2% recoverable strain at 50 MPa when they were heat treated at 1277 °C for 10 h and subsequently aged at 600 °C for 4 h. However, a large irrecoverable strain was observed when the applied stress was 100 MPa. The sample fractured at a stress level of 150 MPa. Tseng et al. [40] investigated the microstructure of FeNiCoAlTiNb alloy and found the homogeneous solution heat treatment condition was 1277 °C for 24 h. Second phases were formed in the sample when the heat treatment temperature was above 1300 °C.

In this study, Fe₄₁Ni₂₈Co₁₇Al_{11.5}(Ti+Nb)_{2.5} (at.%) polycrystalline alloys that underwent cold rolling were first investigated for their microstructure, texture, thermo- magnetization and shape memory properties using the three-point bending test. In this paper, we

discuss the aging effect on microstructure, transformation temperatures and shape memory properties in the three-point bending test.

2. Materials and Methods

Iron, cobalt, nickel, aluminum, niobium and titanium (99.9 wt%) were used as raw materials. Ingots with the nominal composition of $\text{Fe}_{41}\text{Ni}_{28}\text{Co}_{17}\text{Al}_{11.5}(\text{Ti}+\text{Nb})_{2.5}$ (at.%) were fabricated by vacuum induction melting (VIM). Wire electrical discharge machining (EDM) was used to cut the bar to the desired block, the dimensions of which were $100 \times 25 \times 25$ mm (length, width and thickness). The block was used for the cold-rolling experiment.

As-received $\text{Fe}_{41}\text{Ni}_{28}\text{Co}_{17}\text{Al}_{11.5}(\text{Ti}+\text{Nb})_{2.5}$ (at.%) ingots were prepared using several conditions of thermo-mechanical processing to obtain polycrystalline sheets. The processing conditions are listed below:

- (1) Solution heat treatment (SHT 1) at 1277°C for 24 h (h), followed by water quench (WQ). The first stage of solution heat treatment was used to homogenize the alloys;
- (2) Cold rolling (CR) at room temperature with a reduction ratio of 97% to a thickness of 0.7 mm, and three-point bending samples were cut from the cold-rolled sheet;
- (3) Solution heat treatment (SHT 2) at 1277°C for 1h and water quenching;
- (4) Aging or precipitation heat treatment (PHT) at 600°C for 24, 48 and 72h to introduce L_{12} precipitates and water quenching. For the sake of brevity, we refer to the alloys aged at 600°C for x hours as “ $600^\circ\text{C}-\text{h}$ ”.

The thermo-mechanical processing setup used in this study is summarized in Figure 1.

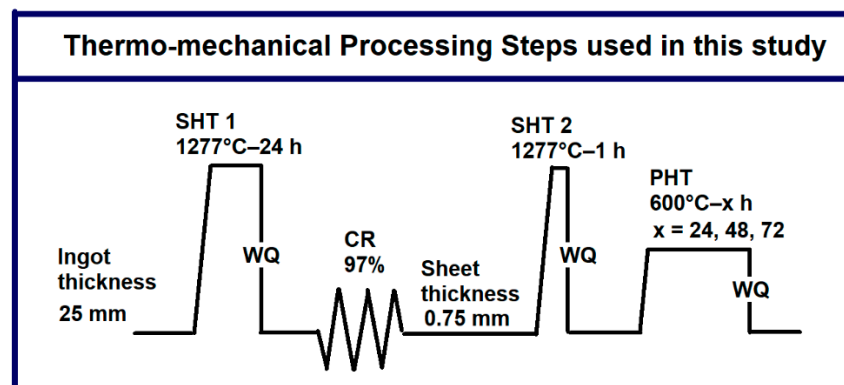


Figure 1. Illustration of the thermo-mechanical processes to obtain $\text{Fe}_{41}\text{Ni}_{28}\text{Co}_{17}\text{Al}_{11.5}(\text{Ti}+\text{Nb})_{2.5}$ (at.%) alloy sheets. SHT 1, WQ, CR, SHT 2 and AHT indicate first stage of solution heat treatment, water quenching, cold rolling, second stage of solution heat treatment and aging heat treatment, respectively.

The FeNiCoAlTiNb alloys were ground to $0.05\ \mu\text{m}$ and the surfaces were etched with the solution, which was composed of 7% nitric acid and 93% ethanol. The observation of microstructure was made using the Olympus digital optical microscope. Vickers microhardness measurements were made using a microhardness tester FM-310. The samples for the OM tests were (1) 97%CR + $1277^\circ\text{C}-1\ \text{h}$, (2) 97%CR + $1277^\circ\text{C}-1\ \text{h}$ + $600^\circ\text{C}-24\ \text{h}$, (3) 97%CR + $1277^\circ\text{C}-1\ \text{h}$ + $600^\circ\text{C}-48\ \text{h}$ and (4) 97%CR + $1277^\circ\text{C}-1\ \text{h}$ + $600^\circ\text{C}-72\ \text{h}$. Hardness values of measurement were made at room temperature.

A high-resolution X-ray diffractometer with $\text{Cu-K}\alpha$ radiation ($\lambda = 0.1542\ \text{nm}$) was used to obtain the crystal structures of $1277^\circ\text{C}-24\ \text{h}$, 97%CR and 97%CR after heat treatment at 1277°C for 1 h samples. The as-received, $1277^\circ\text{C}-24\ \text{h}$, 97%CR and 97%CR samples after heat treatment at 1277°C for 1 h were cut out for texture measurement using a D5000 X-ray diffraction device (Siemens, Aubrey, TX, USA). The $\text{FCC}\{111\}$, $\text{FCC}\{200\}$, and $\text{FCC}\{220\}$ pole figure data were selected to plot the orientation distribution functions (ODFs) [19]. The microstructure and texture of the cold-rolled specimens after being treated with solution at 1277°C for 1h were determined using electron backscatter diffraction (EBSD). The etching solution used in preparing the sample surface was 10% HClO_4 + 90% $\text{C}_2\text{H}_5\text{OH}$.

The SEM images of fractured surfaces for the 600 °C–48 h sample after three-point bending test were obtained using a JSM-7800F device (JEOL, Musashino, Akishima, Tokyo).

In order to find the martensitic transformation temperatures and the thermo-magnetization properties, the cold-rolled samples that were aged at 600 °C for 24, 48 and 72 h were measured by using a superconducting quantum interference device (SQUID) under fields of 0.05 and 7 Tesla. The cooling and heating rate was determined to be 5 K/min. The magnetic results were used to determine the martensitic transformation temperatures used to calculate the temperature hysteresis. The sample was first heated up to 110 °C under a zero magnetic field, and then cooled down to –260 °C and heated up around to 110 °C under a constant magnetic field of 0.05 Tesla. After the 0.05 Tesla test, the magnetic field was increased to 7 Tesla. The sample was cooled from 120 °C to –260 °C and heated up to 120 °C again to complete one cycle. In thermo-magnetization curve, magnetization was used to describe how a material responds to an applied magnetic field and one magnetization (emu/g) corresponded to 1 Am²/kg.

The shape memory effects of FeNiCoAlTiNb samples were determined using the three-point bending method with an ElectroForce 3230 (TA Instruments, New Castle, DE, USA) equipped with a hot/cold chamber. The support span was 20 mm. Three-point bending shape memory samples were cut from the cold-rolled sheet. The samples were solution-treated at 1277 °C for 1 h and underwent aging heat treatment at 600 °C for 24, 48 and 72 h. The samples were straight before the bending test. Figure 2 presents the setup of the bending test. For this test, the sample was first loaded with a stress level of 50 MPa at room temperature and was then cooled and heated between –150 °C and room temperature to complete one thermal cycle. This process was repeated for increasing stress levels. A heating/cooling rate was selected as 5 K/min. When the sample completed one thermal cycle, the applied stress level increased to 100 MPa and the next heating/cooling cycle was carried out. The same procedure was applied using the stress levels of 150 and 200 MPa. The 600 °C–48 h sample failed when the applied stress level was 250 MPa. The 600 °C–72 h sample fractured during the 150 MPa applied stress level.

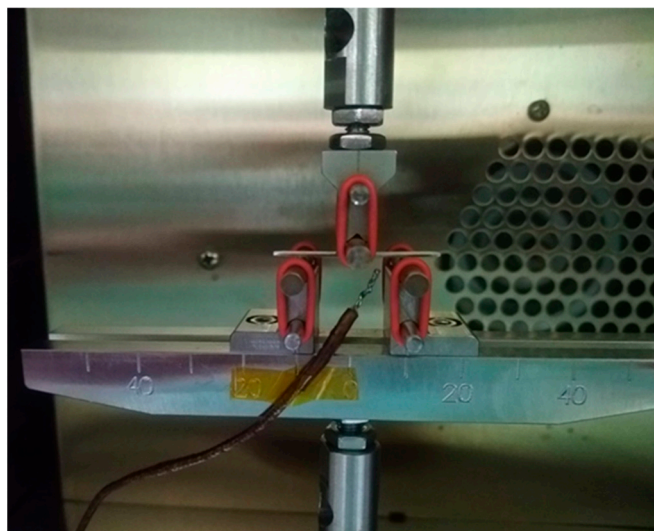


Figure 2. Setup for the bending test.

3. Results

3.1. Microstructure and Microhardness Results

Figure 3a–d show the microstructure of the FeNiCoAlTiNb polycrystalline in different thermo-mechanical processing conditions. Figure 3a shows the 97%CR sample after being heat treated at 1277 °C for 1 h. The grain boundaries were clearly seen in this condition. Figure 3b–d display the 97%CR sample after being treated with solution at 1277 °C for 1 h and aging heat treatment at 600 °C for 24, 48 and 72 h. The microstructure results show that leaf-like β phases accumulate in the grain boundary, especially in triple junctions.

Increasing the aging times from 24 to 72 h, large number of β phases form in the aging sample. The generation of β phases can also be observed in FeNiCoAlXB (X: Ta, Ti, Nb) systems [8–10,12].

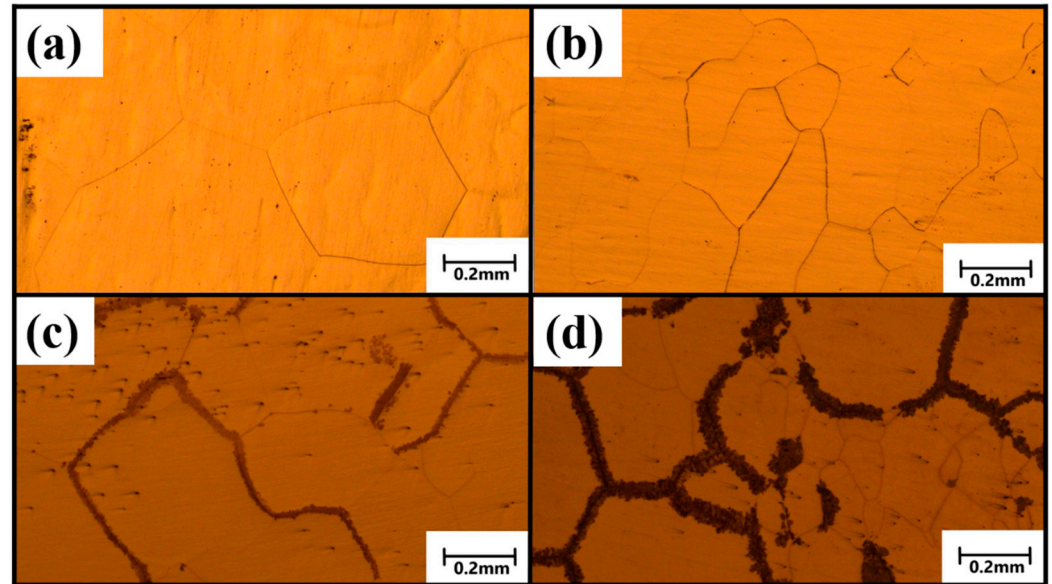


Figure 3. Microstructure of FeNiCoAlTiNb alloy in different thermo-mechanical processing conditions: (a) 97%CR+1277 °C-1 h, (b) 97%CR+1277 °C-1 h + 600 °C-24 h, (c) 97%CR + 1277 °C-1 h + 600 °C-48 h and (d) 97%CR + 1277 °C-1 h + 600 °C-72 h.

Table 1 shows the Vickers microhardness of the FeNiCoAlTiNb alloy in different conditions of thermomechanical processing. The hardness value of the 97%CR sample is around 430HV. After the solution heat treatment, the hardness is 260HV. For the aging heat treatment condition, the microhardness values are 462 HV, 510 HV and 552 HV for 600 °C-24 h, 600 °C-48 h and 600 °C-72 h, respectively. The microhardness results of three aging conditions are summarized in Figure 4. From the results, as the aging times increase, the hardness values increase their values due to the formation of precipitation hardening. In FeNiCoAlTa single crystal studies, the hardness values increased when the aging times increased from 24 to 90 h at an aging temperature of 600 °C, which suggests precipitates strengthen the austenite matrix [21].

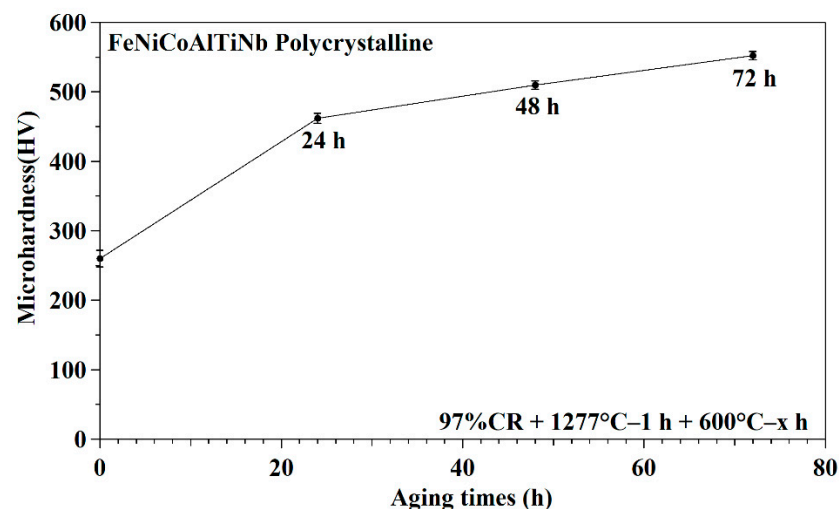


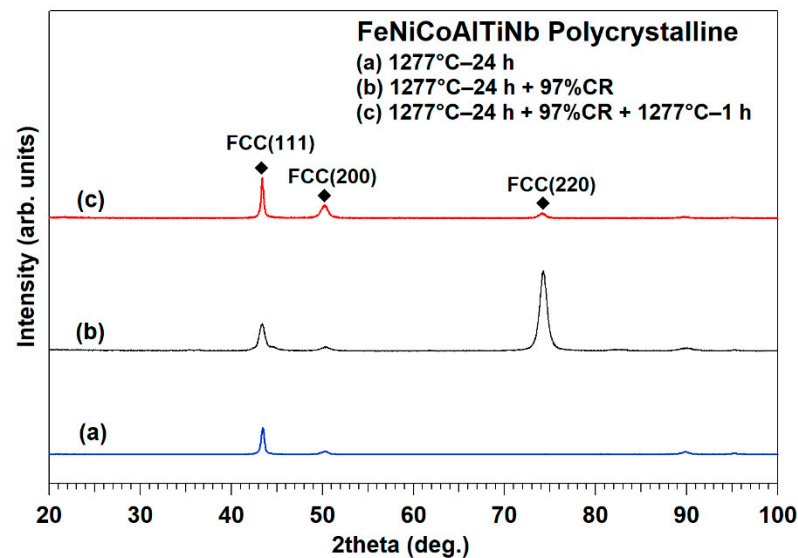
Figure 4. Hardness results of FeNiCoAlTiNb samples under different aging conditions.

Table 1. Microhardness results of FeNiCoAlTiNb alloy in different thermo-mechanical processing conditions.

Thermo-Mechanical Processing	Vickers Hardness (HV)
97%CR	430 ± 12
97%CR + 1277 °C–1 h	260 ± 6.5
97%CR + 1277 °C–1 h + 600 °C–24 h	462 ± 5.5
97%CR + 1277 °C–1 h + 600 °C–48 h	510 ± 5
97%CR + 1277 °C–1 h + 600 °C–72 h	552 ± 6

3.2. XRD Results

Figure 5 presents the XRD results for samples' conditions: 1277 °C–24 h, 1277 °C–24 h + 97%CR and 1277 °C–24 h + 97%CR + 1277 °C–1 h. The XRD profile results show that face-centered cubic (FCC) phases are found in three conditions. In the cold-rolled samples after 1277 °C–1 h treatment, a strong peak intensity is observed in the (111) plane.

**Figure 5.** XRD results of FeNiCoAlTiNb samples under different processing conditions: 1277 °C–24 h, 1277 °C–24 h + 97%CR and 1277 °C–24 h + 97%CR + 1277 °C–1 h.

3.3. Magnetization Results

The transformation temperatures of the cold-rolled samples after being aged at 600 °C for 24, 48 and 72 h were determined using the magnetic field test. After solution heat treatment, the 97% cold-rolled sample does not show here, since martensitic transformation is not observed in this condition. Figure 6a–f display the thermo-magnetization results of FeNiCoAlTiNb that underwent aging heat treatment at 600 °C for 24, 48 and 72 h under the magnetic fields of 0.05 and 7 Tesla. The martensitic transformation temperatures of the sample aged at 600 °C for 24, 48 and 72 h were determined using the magnetic field results of 0.05 Tesla, as shown in Figure 6a,c,e. The tangent line method was used to determine the transformation temperatures. From the result, the martensitic transformation temperatures of the 600 °C–24 h aging sample were: austenite finish temperature (A_f) = –103 °C, austenite start temperature (A_s) = –147 °C, martensite start temperature (M_s) = –135 °C and martensite finish temperature (M_f) = –189 °C. The temperature hysteresis was defined as $\Delta T = |A_f - M_s|$, and was calculated to be 36 °C. For the 600 °C–48 h aging sample, A_f = –68 °C, A_s = –105 °C, M_s = –106 °C and martensite finish temperature (M_f) = –154 °C. The temperature hysteresis was 30 °C. For the 600 °C–72 h aging sample, A_f = –53 °C, A_s = –100 °C, M_s = –90 °C, and martensite finish temperature (M_f) = –134 °C. The temperature hysteresis was 37 °C. The transformation temperatures

and temperature hysteresis of the FeNiCoAlXB (X: Ta, Nb, Ti) alloys and the FeNiCoAlTiNb alloy reported by the present authors [8–10] are summarized in Table 2.

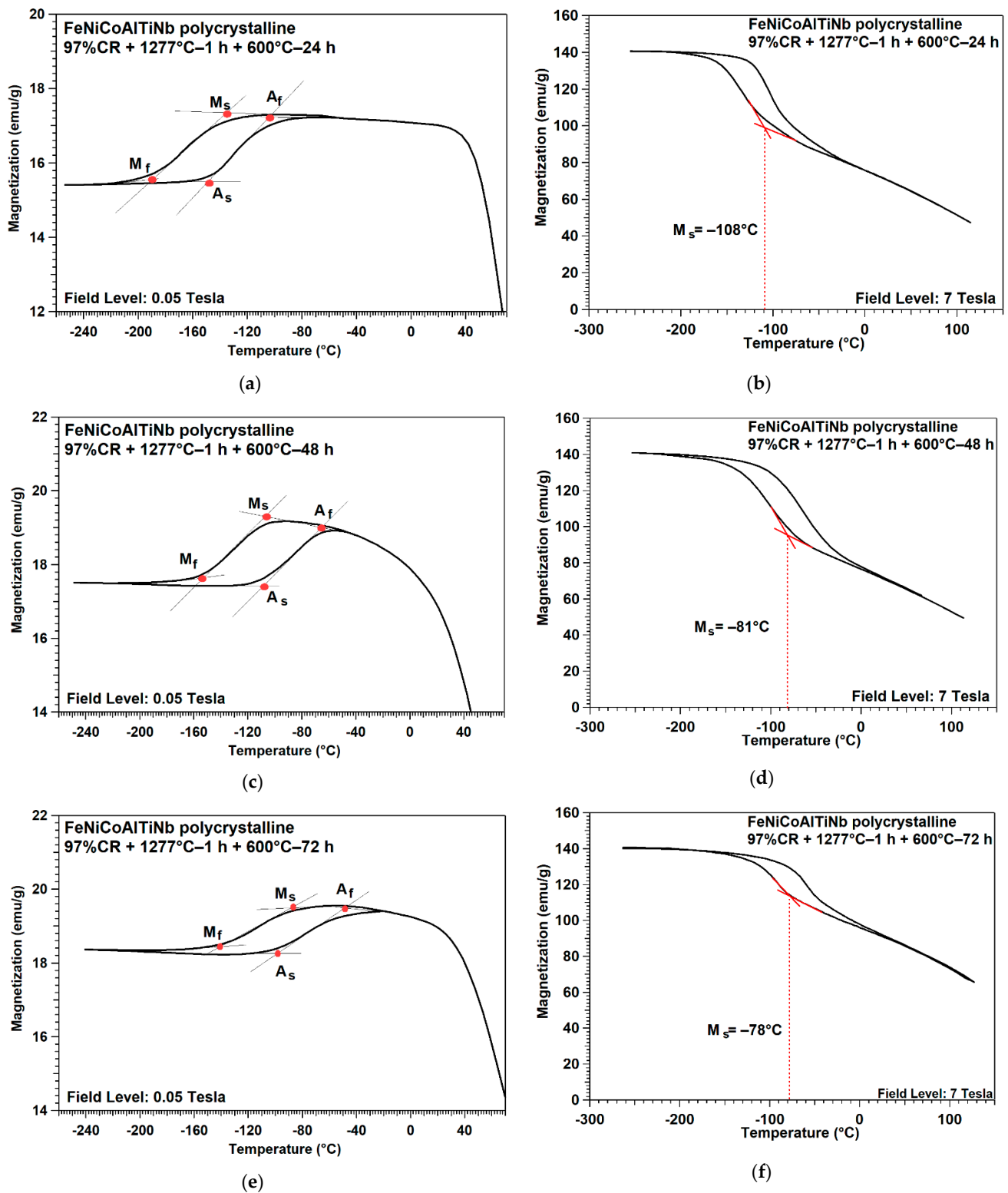


Figure 6. Thermo-magnetization curves of FeNiCoAlTiNb aging sample. (a,b) 0.05 and 7 Tesla for 600 °C–24 h, (c,d) 7 Tesla for 600 °C–48 h, (e,f) 0.05 and 7 Tesla for 600 °C–72 h.

Figure 6b,d,f present the magnetic results of the 7 Tesla experiments; the magnetization of both aging conditions is 140 emu/g. The M_s can also be obtained using tangent line

methods, and M_s was $-108\text{ }^\circ\text{C}$, $-81\text{ }^\circ\text{C}$ and $-78\text{ }^\circ\text{C}$ in $600\text{ }^\circ\text{C}$ -24 h, $600\text{ }^\circ\text{C}$ -48 h and $600\text{ }^\circ\text{C}$ -72 h conditions, respectively. The results show the transformation temperatures move to higher temperatures as the aging times increase. A similar trend was reported in FeNiCoAlTa single crystals [21].

Table 2. Transformation temperatures and temperature hysteresis of the present FeNiCoAlTiNb alloy in comparison with data for FeNiCoAlXB (X: Ta, Nb, Ti) alloys [8–10].

Alloys	Transformation Temperature ($^\circ\text{C}$)	Temperature Hysteresis ($^\circ\text{C}$)
FeNiCoAlTaB (600 $^\circ\text{C}$ -72 h)	Af = -62 and $M_s = -86$	24
FeNiCoAlTa (600 $^\circ\text{C}$ -90 h)	Af = -63 and $M_s = -98$	35
FeNiCoAlNbB (600 $^\circ\text{C}$ -80 h)	Af = -30 and $M_s = -70$	40
FeNiCoAlTiB (550 $^\circ\text{C}$ -24 h)	Af = -4 and $M_s = -35$	31
FeNiCoAlTiNb (600 $^\circ\text{C}$ -24 h)	Af = -103 and $M_s = -135$	36
FeNiCoAlTiNb (600 $^\circ\text{C}$ -48 h)	Af = -68 and $M_s = -106$	32
FeNiCoAlTiNb (600 $^\circ\text{C}$ -72 h)	Af = -53 and $M_s = -90$	37

3.4. EBSD and ODFs Results

The recrystallization texture of the 97% cold-rolled samples after undergoing solution treatments at $1277\text{ }^\circ\text{C}$ for 1 h was obtained using EBSD. Figure 7 shows a quasi-colored orientation map of the 97% cold-rolled samples after solution treatment, where the color indicates the crystal orientation presented in the stereographic triangle. In the figure, the RD, TD and ND represent the rolling direction, transverse direction and normal direction, respectively. From the results of orientation maps, the average grain size is around $402\text{ }\mu\text{m}$. In the FeNiCoAlTaB alloy, the average grain size is around $400\text{ }\mu\text{m}$ [8]. From the inverse pole figure result, strong $\langle 001 \rangle$ orientation is observed in the rolling direction. The intensity of texture is 13.64. The recrystallization texture of the present alloy is similar to the $\langle 100 \rangle$ texture of the FeNiCoAlTaB and FeNiCoAlTiB alloy [8,10] but different from the $\langle 110 \rangle$ texture of the Fe–Ni–Co–Al–Nb–B alloy [9].

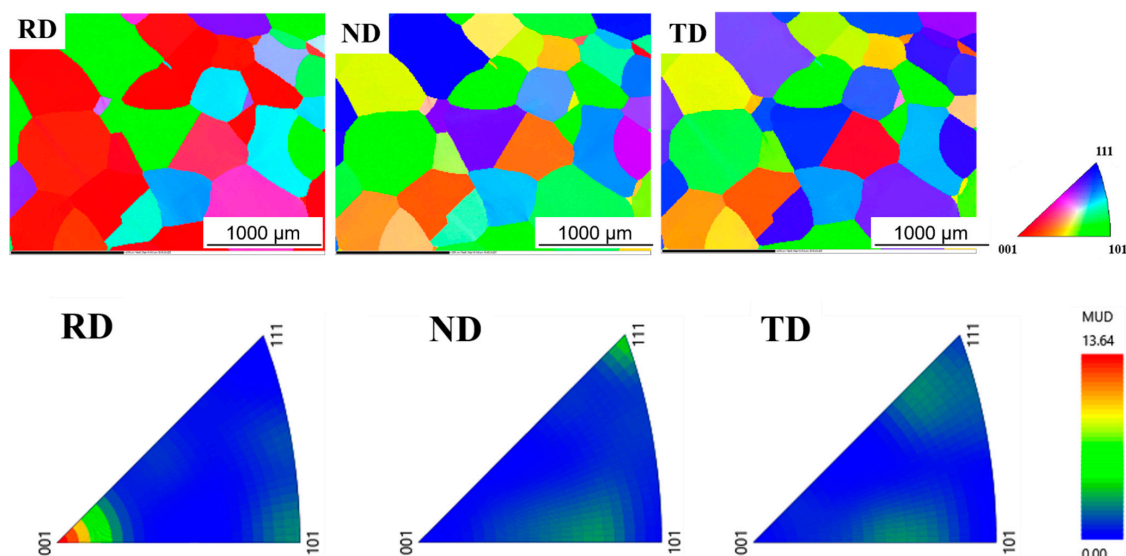


Figure 7. Quasi-colored orientation maps of microstructure and inverse pole figures of the cold-rolled alloy after being solution treated at $1277\text{ }^\circ\text{C}$ for 1 h (RD: rolling direction, TD: transverse direction, ND: normal direction).

Figure 8 shows ODFs ($\phi_2 = 0^\circ, 45^\circ, \text{ and } 60^\circ$ sections) for the alloy with different thermo-mechanical processing conditions. The texture of the as-received sample is cubic $\{001\}\langle 100\rangle$, Goss/brass (G/B) $\{110\}\langle 115\rangle$ and brass ($\{110\}\langle 112\rangle$). The sample after solution treatment shows cubic $\{001\}\langle 100\rangle$, rotated cube (Rt-C) $\{001\}\langle 110\rangle$ and rotated Cu (Rt-Cu) $\{112\}\langle 011\rangle$ texture. The 97% cold-rolled sample shows Goss (G) $\{110\}\langle 001\rangle$ and Goss/brass (G/B) $\{110\}\langle 115\rangle$ textures. The cold-rolled sample that underwent 1277C–1h heat treatment shows a Goss (G) $\{110\}\langle 001\rangle$ texture. Therefore, cold-rolling deformation and recrystallization at 1277 for 1h give rise to a preferred $\langle 100\rangle$ recrystallized orientation.

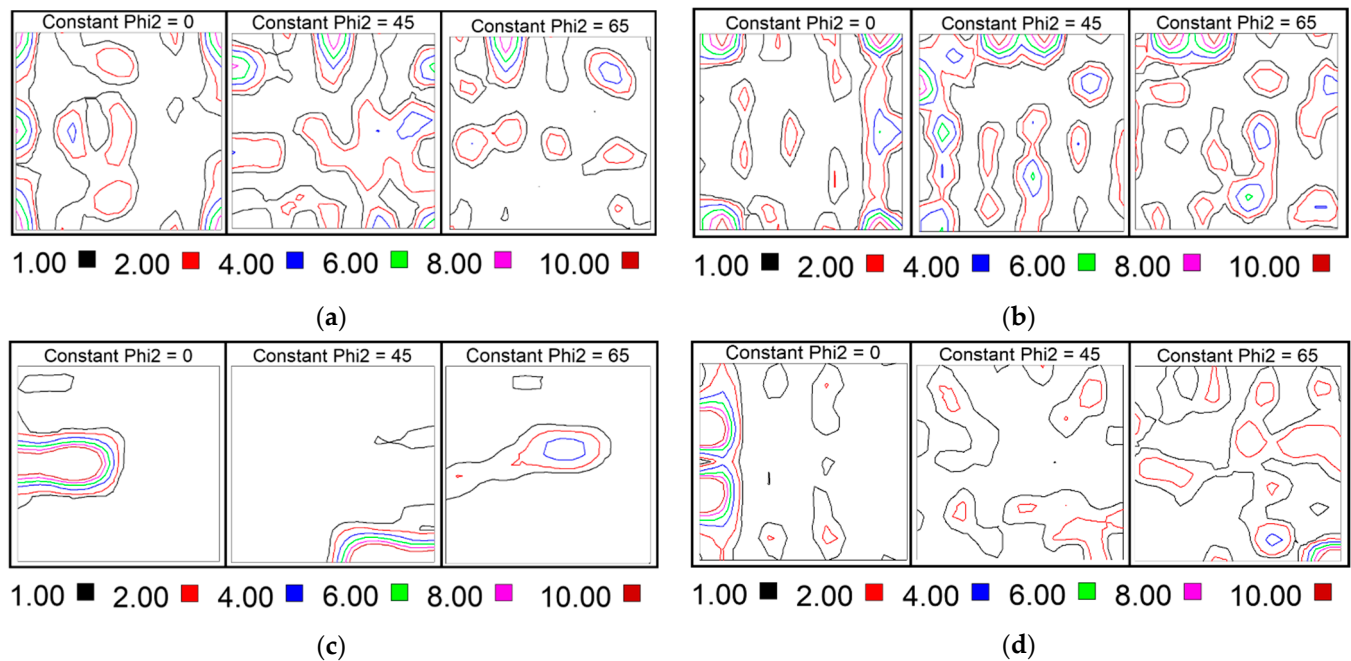


Figure 8. ODFs results of FeNiCoAlTiNb polycrystalline under different thermo-mechanical processing conditions: (a) as-received, (b) 1277C–24 h, (c) 97%CR and (d) 97%CR + 1277 °C for 1 h.

3.5. Three-Point Bending Test Results

The results from the thermal cycling under the three-point bending test at different stress levels are displayed in Figure 9. Figure 9a shows the thermal cycling results of sample aged at 600 °C for 24 h. When the stress level is 100 MPa, the martensitic transformation occurs at around -150°C . The complete loop of phase transformation does not observe because the transformation temperature is too low, and the device can only cool down to -150°C , and the stress level is not high enough to induce martensitic transformation to higher temperature. The sample fails during the 200 MPa thermal cycle test. The early failure of thermal cycling specimens was probably caused by the variant–variant interactions during transformation process. During the cooling process, the interaction between the growing martensitic phase increases variant interaction and leads to fracture [20].

Figure 9b presents the thermal cycling results of the sample aged at 600 °C for 48 h. The phase transformation was observed when the stress level was 50 MPa. The sample failed when the stress level increased to 250 MPa. Transformation temperatures, recoverable strain and temperature hysteresis values can be obtained through this test. The maximum recoverable strain was around 1.6% at a stress level of 200 MPa. The transformation temperatures (A_f and M_s) are extracted in Figure 9b and plotted as a function of applied stress, as shown in Figure 9c. From the results, when the applied stress levels increased, the A_f and M_s slightly increased their temperatures. The M_s was -110°C at 50 MPa and increased to -100°C at 200 MPa. The A_f was -70°C at 50 MPa and increased to -56°C at 200 MPa. In addition, the lines for each transformation temperature could be extrapolated down to zero stress to determine the stress-free transformation temperatures. The M_s was

–112 °C and Af was –74 °C, which were values close to the transformation temperatures determined by the SQUID results.

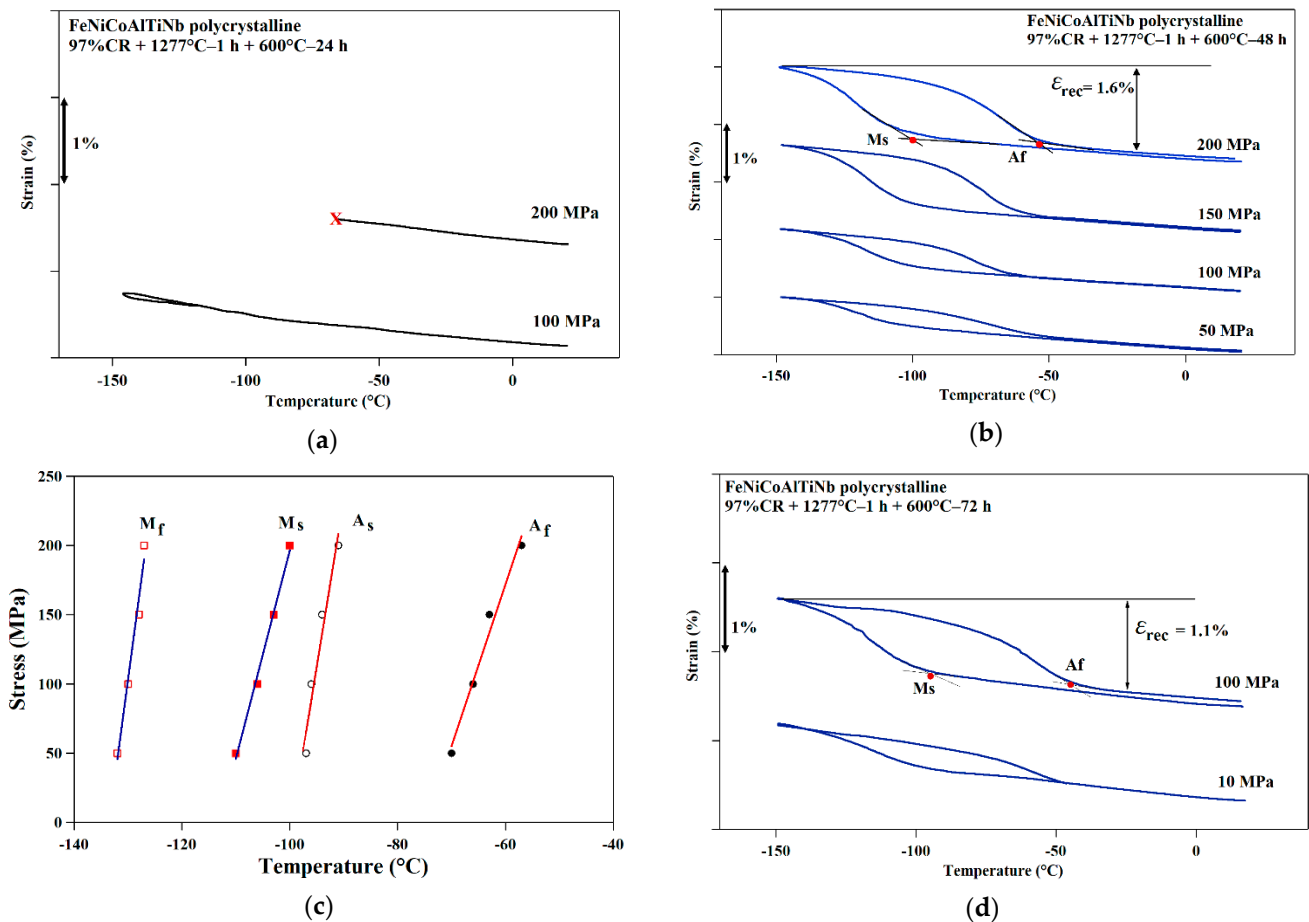


Figure 9. Shape memory effect of FeNiCoAlTiNb 97% cold-rolled sample after being aged at 600 °C for x hours using three-point bending test. (a) 600 °C–24 h aging sample, (b) 600 °C–48 h aging sample, (c) stress versus temperature phase diagram for a 600 °C–48 h aging sample. The values for each transformation temperature are obtained from Figure 7b results. (d) 600 °C–72 h aging sample.

Figure 9d displays the thermal cycling results of the sample aged at 600 °C for 72 h. The maximum recoverable strain was 1.1%. The sample failed during the 150 MPa thermal cycle test. The sample was brittle due to the formation of β phases at the grain boundaries.

4. Discussion

From the three-point bending test results, it is clear that the recoverable strain of the 600 °C–48 h aged sample is smaller than the theoretical calculated values of FeNiCoAlTaB [8]. One possible reason for this is the smaller fraction of low angle grain boundary (LAB). Figure 10 shows the grain boundary misorientation of the 97% cold-rolled alloy after solution treatment at 1277 °C for 1 h. Based on the calculation, the fraction of LABs is about 11%. The FeNiCoAlTiNb polycrystalline alloy systems are required to undergo aging heat treatment to increase the strength of the austenite matrix and obtain the nano size L_{12} precipitates [8–10,25]. Meanwhile, β phases (grain boundary precipitates) are generated along the grain boundary, especially at the triple junction. β phases prefer to form at high angle grain boundaries (HABs) due to higher energy [9,10]. From Figure 3c results, it is seen that the β phases form at the grain boundaries. As the fraction of LABs is 11% in the 97% cold-rolled sample after solution treatment at 1277 °C for 1 h, β phases can be seen in the grain boundaries for the 600 °C–48 h sample. β phases deteriorate ductility and shape memory properties. As a consequence, the recoverable strain of the

shape memory effect is smaller than the theoretical calculated values. Although a small number of β phases is formed in the 600 °C–24 sample, the transformation curve of the shape memory effect is not observed even under the 2000 MPa stress level due to its lowest transformation temperatures. For the 600 °C–72 sample, more β phases were generated in this aging condition, as shown in Figure 3d. As a consequence, the sample failed during the 150 MPa test.

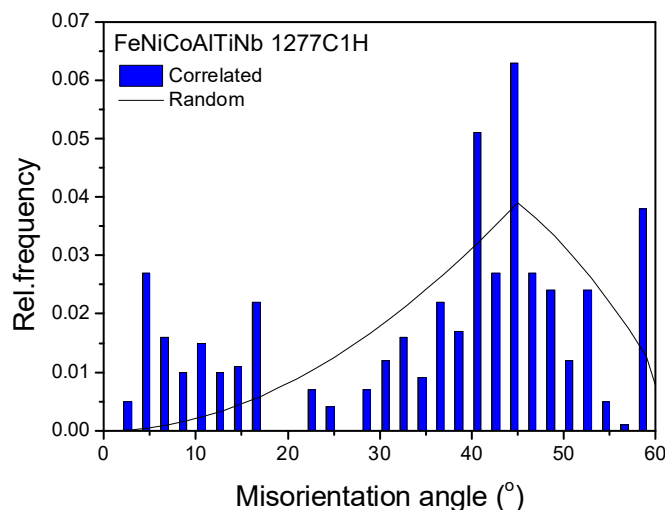


Figure 10. Grain boundary misorientation of the cold-rolled alloy after solution treatment.

Another possible reason for the significantly lower shape memory recoverable strain observed in this study is related to the texture intensity of the $\langle 100 \rangle$ orientation in the rolling direction. In this study, the texture intensity of the $\langle 100 \rangle$ component in the RD direction is 13.64, as shown in Figure 7. The texture intensity of same component and orientation in FeNiCoAlTaB is 25.4 [8]. The value of texture intensity in this sample is lower than that in the FeNiCoAlTaB specimen. Texture development can improve the recoverable strain of shape memory and superelasticity [8–10]. In iron-based SMAs, reducing the grain constraint is crucial due to martensite variant selection. Based on the Bain distortion theory, only three variants can assist the deformation, which is different from the NiTi SMAs, in which twenty-four variants are able to assist deformation [1].

In iron-based SMAs, the theoretical transformation strains are 8.7%, 4.1% and 2.1% in $\langle 100 \rangle$, $\langle 110 \rangle$ and $\langle 111 \rangle$ orientations, respectively [8]. Based on the results in Figure 7, Quasi-colored orientation maps in the rolling direction show that some grains are oriented in the $\langle 110 \rangle$ and $\langle 111 \rangle$ direction. The large difference in the crystal orientation between surrounding grains increases the grain constraint. When the applied stress level is increased, the incompatibility between adjacent grains becomes intense and results in the deterioration of ductility. Figure 11a presents SEM images of the fracture surface for the 600 °C–48 h sample after three-point bending test. The fracture is along the grain boundary. Figure 11b shows an SEM image of a cross section. The fracture surfaces of the sample are smooth. The results suggest that the sample has a brittle intergranular fracture, and the fracture is along a grain boundary.

The final possible reason for the smaller strain of this polycrystalline material is the addition of boron. The volume fraction of LABs is 11% in the present alloy and 11% in FeNiCoAlNbB [9]. Since both alloys have a similar fraction of LABs, the aging condition for the FeNiCoAlNbB alloy is 600 °C for 96 h. A small amount of grain boundary precipitates is observed in this aging condition. Since B element tends to lower the grain boundary energy, this retards β phases' growth in the FeNiCoAlNbB alloy. The recrystallization texture of the FeNiCoAlNbB alloy near $\langle 110 \rangle$ in the rolling direction is different from the FeNiCoAlTaB [8,9] and present alloy.

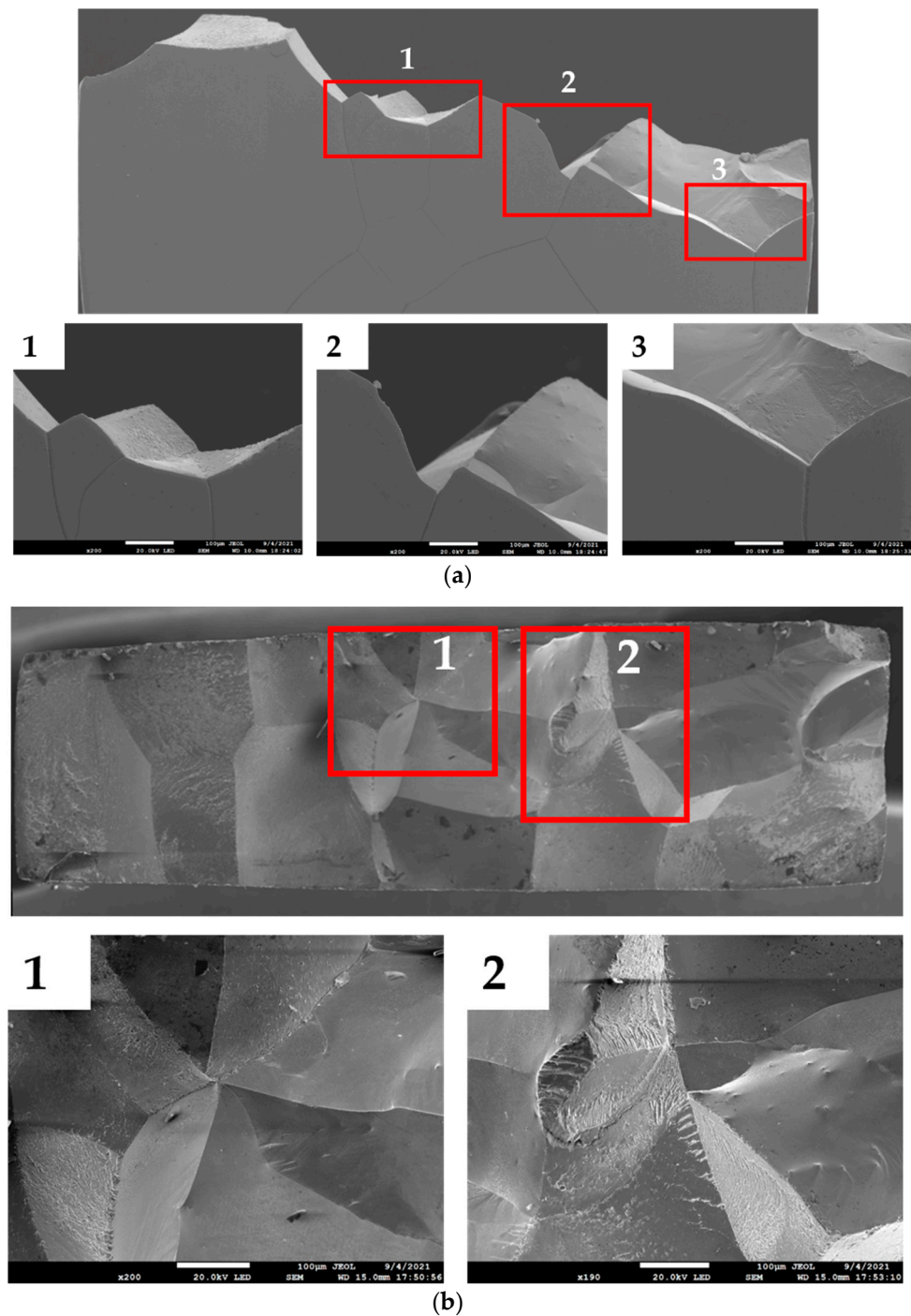


Figure 11. SEM images of 600 °C–48 h sample after three-point bending test. (a) Fracture surface of sample and (b) cross section of fracture surface.

5. Conclusions

In summary, the microstructure, thermo-magnetization, and shape memory properties of new cold-rolled FeNiCoAlTiNb SMA samples were investigated for the first time. The main conclusions can be listed as follows:

- (1) The β phases were generated along the grain boundaries when the aging times were 48 and 72 h at 600 °C. The XRD results of cold-rolled samples after 1277 °C–1 h showed a strong peak intensity in the (111) plane.
- (2) The cold-rolled sample aged at 600 °C for 24, 48 and 72 h showed phase transformation under the magnetic field of 0.05 and 7 Tesla. As the aging durations were

increased from 24 to 72 h, the martensitic transformation temperature shifted to a higher temperature, which indicates the transformation temperatures increase with an increase in the aging times.

- (3) Recrystallization textures of near $\langle 100 \rangle$ orientation were developed using a combination of cold rolling with a reduction ratio of 97% and subsequent annealing at 1277 °C for 1 h. The average grain size was around 400 μm , and the intensity of texture was 13.64.
- (4) Shape memory behavior was not observed in the 600 °C–24 h sample at a 2000 MPa stress level due to the fact that it possessed the lowest transformation temperature. The shape memory properties in the 600 °C–48 h sample with a recoverable strain of 1.6% at 200 MPa stress level were obtained using a three-point bending test. The observed recoverable strain values were lower than the theoretical values, possibly owing to the smaller fraction of low angle grain boundary, the formation of grain boundary precipitates and grain boundary constraint due to a slightly lower than expected intensity of texture in the samples. The thermal hysteresis was around 40 °C. The recoverable strain in the 600 °C–72 h sample was 1.1% at 100 MPa. The sample fractured at a stress level of 150 MPa due to the formation of a large amount of brittle β phases.

Author Contributions: Conceptualization, L.-W.T.; methodology, L.-W.T. and C.-H.C.; validation, L.-W.T. and C.-H.C.; investigation, L.-W.T., C.-H.C., W.-C.C., Y.C. and N.-H.L.; resources, L.-W.T. and C.-H.C.; data curation, W.-C.C., Y.C. and N.-H.L.; writing—original draft preparation, L.-W.T.; writing—review and editing, L.-W.T.; visualization, L.-W.T. and C.-H.C.; supervision, L.-W.T.; project administration, L.-W.T. All authors have read and agreed to the published version of the manuscript.

Funding: This research was funded by the Ministry of Science and Technology (MOST), grant numbers MOST 109-2221-E-018-010-MY2. This work was financially supported by the Young Scholar Fellowship Program of the Ministry of Science and Technology (MOST) in Taiwan, grant number MOST 110-2636-E-002-005.

Acknowledgments: The FeNiCoAlTiNb alloys were fabricated by the National Chung-Shan Institute of Science and Technology (NCSIST), which is gratefully acknowledged. The authors would like to thank Yung-Sheng Chen at the Instrumentation Center, National Tsing Hua University for the SQUID measurements. Thanks Ko-Kai Tseng at the High Entropy Materials Center, National Tsing Hua University for the cold rolling experiment.

Conflicts of Interest: The authors declare no conflict of interest.

References

1. Otsuka, K.; Wayman, C.M. *Shape Memory Materials*; Cambridge University Press: Cambridge, UK, 1998; pp. 117–132.
2. Jani, J.M.; Leary, M.; Subic, A.; Gibson, M.A. A review of shape memory alloy research, applications and opportunities. *Mater. Des.* **2014**, *56*, 1078–1113. [[CrossRef](#)]
3. Omori, T.; Kainuma, R. Martensitic transformation and superelasticity in Fe-Mn-Al-Based shape memory alloys. *Shape Mem. Superelasticity* **2017**, *3*, 334–355. [[CrossRef](#)]
4. Khalil, W.; Mikolajczak, A.; Bouby, C.; Zineb, T.B. A constitutive model for Fe-based shape memory alloy considering martensitic transformation and plastic sliding coupling: Application to a finite element structural analysis. *J. Intell. Mater. Syst. Struct.* **2012**, *23*, 1143–1160. [[CrossRef](#)]
5. Maki, T.; Kobayashi, K.; Minato, M.; Tamura, I. Thermoelastic martensite in an ausaged Fe-Ni-Ti-Co alloy. *Scr. Metall.* **1984**, *18*, 1105–1109. [[CrossRef](#)]
6. Sehitoglu, H.; Karaman, I.; Zhang, X.; Chumlyakov, Y.; Maier, H.J. Deformation of FeNiCoTi shape memory single crystals. *Scr. Mater.* **2001**, *44*, 779–784. [[CrossRef](#)]
7. Sehitoglu, H.; Zhang, X.Y.; Kotil, T.; Canadinc, D.; Chumlyakov, Y.; Maier, H.J. Shape memory behavior of FeNiCoTi single and polycrystals. *Metall. Mater. Trans. A* **2002**, *33*, 3661–3672. [[CrossRef](#)]
8. Tanaka, Y.; Himuro, Y.; Kainuma, R.; Sutou, Y.; Omori, T.; Ishida, K. Ferrous polycrystalline shape-memory alloy showing huge superelasticity. *Science* **2010**, *27*, 1488–1490. [[CrossRef](#)]
9. Omori, T.; Abe, S.; Tanaka, Y.; Lee, D.; Ishida, K.; Kainuma, R. Thermoelastic martensitic transformation and superelasticity in Fe-Ni-Co-Al-Nb-B polycrystalline alloy. *Scr. Mater.* **2013**, *69*, 812–815. [[CrossRef](#)]

10. Lee, D.; Omori, T.; Kainuma, K. Ductility enhancement and superelasticity in Fe-Ni-Co-Al-T-B polycrystalline alloy. *J. Alloy. Compd.* **2014**, *617*, 120–123. [[CrossRef](#)]
11. Otsuka, H.; Yamada, H.; Maruyama, T.; Tanahashi, H.; Matsuda, S.; Murakami, H. Effects of alloying additions on Fe-Mn-Si shape memory alloys. *ISIJ Int.* **1990**, *30*, 674–679. [[CrossRef](#)]
12. Sato, A.; Chishima, E.; Yamaji, Y.; Mori, T. Orientation and composition dependencies of shape memory effect in Fe-Mn-Si Alloys. *Acta Metall.* **1984**, *32*, 539–547. [[CrossRef](#)]
13. Ando, K.; Omori, T.; Ohnuma, T.; Kainuma, R.; Ishida, K. Ferromagnetic to weak-magnetic transition accompanied by bcc to fcc transformation in Fe-Mn-Al alloy. *Appl. Phys. Lett.* **2009**, *95*, 212504. [[CrossRef](#)]
14. Omori, T.; Watanabe, K.; Umetsu, R.Y.; Kainuma, R.; Ishida, K. Martensitic transformation and magnetic field-induced strain in Fe-Mn-Ga shape memory alloy. *Appl. Phys. Lett.* **2009**, *95*, 082508. [[CrossRef](#)]
15. Zhu, W.; Liu, E.K.; Feng, L.; Tang, X.D.; Chen, J.L.; Wu, G.H.; Liu, H.Y.; Meng, F.B.; Luo, H.Z. Magnetic-field-induced transformation in FeMnGa alloys. *Appl. Phys. Lett.* **2009**, *95*, 222512. [[CrossRef](#)]
16. Omori, T.; Ando, K.; Okano, M.; Xu, X.; Tanaka, Y.; Ohnuma, I.; Kainuma, R.; Ishida, K. Superelastic effect in polycrystalline ferrous alloys. *Science* **2011**, *333*, 68–71. [[CrossRef](#)] [[PubMed](#)]
17. Sawaguchi, T.; Maruyama, T.; Otsuka, H.; Kushibe, A.; Inoue, Y.; Tsuzaki, K. Design concept and applications of Fe-Mn-Si-based alloys -from shape-memory to seismic response control. *Mater. Trans.* **2016**, *57*, 283–293. [[CrossRef](#)]
18. Geng, Y.; Lee, D.; Xu, X.; Nagasako, M.; Jin, X.; Omori, T.; Kainuma, R. Coherency of ordered γ' precipitates and thermoelastic martensitic transformation in FeNiCoAlTaB alloys. *J. Alloy. Compd.* **2015**, *628*, 287–292. [[CrossRef](#)]
19. Fu, H.; Zhao, H.; Shilei, S.; Zhang, Z.; Xie, J. Evolution of the cold-rolling and recrystallization textures in FeNiCoAlNb shape memory alloy. *J. Alloy. Compd.* **2016**, *628*, 287–292. [[CrossRef](#)]
20. Ma, J.; Kockar, B.; Evirgen, A.; Karaman, I.; Luo, Z.; Chumlyakov, Y. Shape memory behavior and tension–compression asymmetry of a FeNiCoAlTa single-crystalline shape memory alloy. *Acta Mater.* **2012**, *60*, 2186–2195. [[CrossRef](#)]
21. Ma, J.; Hornbuckle, B.; Karaman, I.; Thompson, G.B.; Luo, Z.; Chumlyakov, Y. The effect of nanoprecipitates on the superelastic properties of FeNiCoAlTa shape memory alloy single crystals. *Acta Mater.* **2013**, *61*, 3445–3455. [[CrossRef](#)]
22. Krooß, P.; Holzweissig, M.J.; Niendorf, T.; Somsen, C.; Schaper, M.; Chumlyakov, Y.I.; Maier, H.J. Thermal cycling behavior of an aged FeNiCoAlTa single-crystal shape memory alloy. *Scr. Mater.* **2014**, *81*, 28–31. [[CrossRef](#)]
23. Tseng, L.W.; Ma, J.; Karaman, I.; Wang, S.J.; Chumlyakov, Y. Superelastic response of the FeNiCoAlTi single crystals under tension and compression. *Scr. Mater.* **2015**, *101*, 1–4. [[CrossRef](#)]
24. Chumlyakov, Y.I.; Kireeva, I.V.; Kutz, O.A.; Turabi, A.S.; Karaca, H.E.; Karaman, I. Unusual reversible twinning modes and giant superelastic strains in FeNiCoAlNb single crystals. *Scr. Mater.* **2016**, *119*, 43–46. [[CrossRef](#)]
25. Choi, W.S.; Pang, E.L.; Choi, P.P.; Schuh, C.A. FeNiCoAlTaB superelastic and shape-memory wires with oligocrystalline grain structure. *Scr. Mater.* **2020**, *188*, 1–5. [[CrossRef](#)]
26. Abuzaid, W.; Sehitoglu, H. Shape memory effect in FeMnNiAl iron-based shape memory alloy. *Scr. Mater.* **2019**, *169*, 57–60. [[CrossRef](#)]
27. Vollmer, M.; Arold, T.; Kriegel, M.J.; Klemm, V.; Degener, S.; Freudenberger, J.; Niendorf, T. Promoting abnormal grain growth in Fe-based shape memory alloys through compositional adjustments. *Nat. Commun.* **2019**, *10*, 2337. [[CrossRef](#)]
28. Omori, T.; Okano, M.; Kainuma, R. Effect of grain size on superelasticity in Fe-Mn-Al-Ni shape memory alloy wire. *APL Mater.* **2013**, *1*, 032103. [[CrossRef](#)]
29. Ozcan, H.; Ma, J.; Wang, S.J.; Karaman, I.; Chumlyakov, Y.; Brown, J.; Noebe, R.D. Effects of cyclic heat treatment and aging on superelasticity in oligocrystalline Fe-Mn-Al-Ni shape memory alloy wires. *Scr. Mater.* **2017**, *134*, 66–70. [[CrossRef](#)]
30. Ozcan, H.; Ma, J.; Karaman, I.; Chumlyakov, Y.I.; Santamarta, R.; Brown, J.; Noebe, R.D. Microstructural design considerations in Fe-Mn-Al-Ni shape memory alloy wires: Effects of natural aging. *Scr. Mater.* **2018**, *142*, 153–157. [[CrossRef](#)]
31. Tseng, L.W.; Ma, J.; Wang, S.J.; Karaman, I.; Kaya, M.; Luo, Z.P.; Chumlyakov, Y.I. Superelastic response of a single crystalline FeMnAlNi shape memory alloy under tension and compression. *Acta Mater.* **2015**, *89*, 374–383. [[CrossRef](#)]
32. Tseng, L.W.; Ma, J.; Hornbuckle, B.; Karaman, I.; Thompson, G.B.; Luo, Z.; Chumlyakov, Y. The effect of precipitates on the superelastic response of [100] oriented FeMnAlNi single crystals under compression. *Acta Mater.* **2015**, *97*, 234–244. [[CrossRef](#)]
33. Zhang, C.; Zhu, C.; Shin, S.; Casalena, L.; Vecchio, K. Multifunctional non-equiatomic high entropy alloys with superelastic, high damping, and excellent cryogenic properties. *Adv. Eng. Mater.* **2019**, *21*, 1800941. [[CrossRef](#)]
34. Czerny, M.; Cios, G.; Maziarz, W.; Chumlyakov, Y.; Chulist, R. Studies on the two-step aging process of Fe-based shape memory single crystals. *Materials* **2020**, *13*, 1724. [[CrossRef](#)]
35. Czerny, M.; Maziarz, W.; Cios, G.; Wojcik, A.; Chumlyakov, Y.I.; Schell, N.; Fitta, M.; Chulist, R. The effect of heat treatment on the precipitation hardening in FeNiCoAlTa single crystals. *Mater. Sci. Eng. A* **2020**, *784*, 139327. [[CrossRef](#)]
36. Chumlyakov, Y.I.; Kireeva, I.V.; Pobedennaya, P.; Krooß, P.; Niendorf, T. Rubber-like behaviour and superelasticity of [1]-oriented FeNiCoAlNb single crystals containing γ - and β -phase particles. *J. Alloy. Compd.* **2021**, *856*, 158158. [[CrossRef](#)]
37. Chumlyakov, Y.I.; Kireeva, I.V.; Kuksgauzen, D.A.; Niendorf, T.; Krooß, P. Tension-compression asymmetry of the superelastic behavior of high-strength [1]-oriented FeNiCoAlNb crystals. *Mater. Lett.* **2021**, *289*, 129395. [[CrossRef](#)]
38. Chumlyakov, Y.I.; Kireeva, I.V.; Pobedennaya, Z.V.; Krooß, P.; Niendorf, T. Shape memory effect and superelasticity of [1]-oriented FeNiCoAlNb single crystals aged under and without stress. *Metals* **2021**, *11*, 943. [[CrossRef](#)]

-
39. Poklonov, V.; Chumlyakov, Y.; Kireeva, I.; Lyamkind, S. Thermoelastic martensitic transformation in single crystals of FeNiCoAlTiNb alloy. *AIP Conf. Proc.* **2017**, *1909*, 020174.
 40. Tseng, L.W.; Tzeng, Y.C.; Tsai, Y.L.; Chumlyakov, Y.I. Microstructure investigation of new iron-based FeNiCoAlTiNb shape memory alloys. *Results Mater.* **2021**, *10*, 1001881–1001887.